



A new strategy to realize high energy storage properties and ultrafast discharge speed in Sr_{0.7}Bi_{0.2}TiO₃-based relaxor ferroelectric ceramic



Kai Yao^{a,b}, Changrong Zhou^{a,b,*}, Jiang Wang^{a,b}, Qingning Li^a, Changlai Yuan^{a,b}, Jiwen Xu^{a,b}, Guohua Chen^{a,b}, Guanghui Rao^{a,b,*}

^a School of Material Science and Engineering, Guilin University of Electronic Technology, Guilin 541004, Guangxi, People's Republic of China

^b Guangxi Key Laboratory of Information Materials, Guilin University of Electronic Technology, Guilin 541004, Guangxi, People's Republic of China

ARTICLE INFO

Article history:

Received 29 January 2021

Received in revised form 14 June 2021

Accepted 15 June 2021

Available online 18 June 2021

Keywords:

Ergodic relaxor ferroelectrics

Sr_{0.7}Bi_{0.2}TiO₃-based ceramic

Energy storage properties

Charge-discharge performance

ABSTRACT

Although tremendous studies have been focused on dielectric ceramics to achieve excellent energy storage and charge-discharge performance, the dielectric ceramics with high comprehensive energy storage properties for pulsed power applications are still in shortage. The large hysteresis came from domain switching process, severely weaken the energy storage and charge-discharge properties. Here, a strategy through ergodic relaxors with high dynamic polar nanoregions (PNRs) featuring with fast discharge rate and high energy storage efficiency was proposed to achieve high energy storage properties and extremely fast discharge speed in ferroelectric ceramic. The ergodic relaxors of Sr_{0.7}Bi_{0.2}TiO₃ modified by Na_{0.73}Bi_{0.09}NbO₃ (SBT-NBN) ceramics were selected to verify the feasibility of the strategy. Encouragingly, large W_{rec} of 2.49 J/cm³ together with high η of 89.7% can be achieved simultaneously at 250 kV/cm with the composition of 0.96SBT-0.04NBN. The outstanding stability of energy storage characteristics for temperature (25–125 °C) and frequency (1–100 Hz) was also found in 0.96SBT-0.04NBN ceramics. Besides, 0.96SBT-0.04NBN ceramics also possessed an extremely fast discharge rate (~34 ns), remarkable power density P_D (57.3 MW/cm³) as well as high current density C_D (955.4 A/cm²) at 120 kV/cm. This work provided an original strategy for high energy storage efficiency and high power density ceramics in pulse power applications.

© 2021 Elsevier B.V. All rights reserved.

1. Introduction

Dielectric ceramic capacitors are widely utilized in pulsed components and energy storage devices due to their apparent benefits of ultrafast charge/discharge capability, high power density (P_D), and excellent thermal stability, showing huge advantages in weapons, vehicles and power electronics [1–6]. Yet, the relatively low energy storage density and efficiency of dielectric capacitors limit their further applications [2]. Consequently, exploring novel energy storage materials with high energy storage properties has become an urgent issue [4,7]. Generally, the energy storage properties can be calculated by employing polarization–electric field (P–E) loops, expressed by [7]:

$$\text{Energy storage density } W = \int_0^{P_{max}} E dP \quad (1)$$

$$\text{Recoverable energy storage density } W_{rec} = \int_{P_r}^{P_{max}} E dP \quad (2)$$

$$\text{Energy storage efficiency } \eta = \frac{W_{rec}}{W} * 100\% \quad (3)$$

where P , P_{max} , P_r and E denote the polarization, maximum polarization, remnant polarization and applied electric field, respectively. Accordingly, the crucial factors to improve energy storage performance of dielectric capacitors are low P_r , large P_{max} , as well as high breakdown strength (E_B).

Relaxor ferroelectrics have been extensively investigated for energy storage applications owing to the small P_r , and a relative large P_{max} can be induced under a large electric field [8,9]. Sr_{0.7}Bi_{0.2}TiO₃ (SBT), a typical lead-free ergodic relaxor ferroelectric with the perovskite structure, possesses excellent ferroelectric relaxor behavior together with diffused maximum dielectric constant in a wide temperature range, benefiting from Bi³⁺ off centering and Sr site vacancies [10,11]. Furthermore, a high dielectric permittivity can be

* Corresponding authors at: School of Material Science and Engineering, Guilin University of Electronic Technology, Guilin 541004, Guangxi, People's Republic of China

E-mail addresses: zcr750320@guet.edu.cn (C. Zhou), rgh@guet.edu.cn (G. Rao).

obtained in SBT ceramic, which is attributed to dipole polarization related to dipole fluctuation of polar nanoregions (PNRs) [10–12]. However, in the past decades, studies focused on the energy storage performance of (Sr, Bi)TiO₃-based ceramics were rarely reported [10,12,13]. Zhao et al. [10] reported a Sr_{0.7}Bi_{0.2}TiO₃-based relaxor ceramics with high energy storage density of 2.1 J/cm³ and high η of 97.6% at 290 kV/cm. Zhang et al. [12] realized Sr_(1-1.5x)Bi_xTiO₃ ceramics with energy storage density of 1.63 J/cm³ and η of ~61.4% at 217.6 kV/cm. Moreover, (Sr, Bi)TiO₃-based ergodic relaxor ferroelectric ceramics are also a potential candidate for pulsed charge-discharge applications. The ergodic relaxor ferroelectrics with PNRs are converted into unstable ferroelectrics with long-range polar structure under external electric field, and the long-range polar structure will quickly collapse after withdrawing the electric field [5], which lead to a fast discharge rate. Thus a large P_D can be realized due to the stored energy can be released in a short time. Zhao et al. [10] reported fast discharge rate ($\tau_{0.9}$) of 124 ns and high power density of 50.1 MW/cm³ in Sr_{0.7}Bi_{0.2}Ca_{0.1}TiO₃ ceramics. Despite the great achievements made so far, it is necessary to acquire bulk ceramics with good energy storage and charge-discharge performance [14,15].

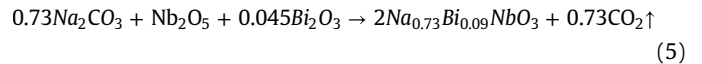
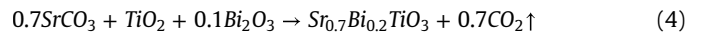
Furthermore, Na_{0.73}Bi_{0.09}NbO₃ was reported to possess good dielectric temperature stability [16–18], as well as decreases P_r and improve E_B [19]. Thus good energy storage performance may be obtained with Na_{0.73}Bi_{0.09}NbO₃ as dopants. Wang et al. [19] reported energy density of 1.56 J/cm³ and high efficiency of 92.5% in (1-x)(0.94Bi_{0.5}Na_{0.5}TiO₃-0.06BaTiO₃)-xNa_{0.73}Bi_{0.09}NbO₃ ceramics. Hu et al. [16] fabricated Bi_{0.5}Na_{0.5}TiO₃-Na_{0.73}Bi_{0.09}NbO₃ ceramics with excellent energy storage density (~2.41 J/cm³) and efficiency (~81.6%) successfully.

Here, the energy storage and charge-discharge properties of (1-x)Sr_{0.7}Bi_{0.2}TiO₃-xNa_{0.73}Bi_{0.09}NbO₃ ((1-x)SBT-xNBN) ceramics were

investigated systematically. The design strategy of this work was shown in Fig. 1. The high dynamic and weak correlation PNRs were supposed to generate by SBT ergodic relaxor ferroelectric ceramics, contributing to the fast discharge rate. The modulation of NBN could effectively reduce the size of PNRs, thus reducing P_r and improving E_B. Finally, a large W_{rec} of 2.49 J/cm³ and a high η of 89.7% were achieved simultaneously in 0.96SBT-0.04NBN ceramics, together with an extremely fast discharge rate of 34 ns and a remarkable P_D of 57.3 MW/cm³. Besides, the W_{rec} displayed good temperature stability over 25–125 °C, as well as excellent frequency stability from 1 to 100 Hz. All the results indicated that (1-x)SBT-xNBN ceramics were promising options for energy storage applications.

2. Experimental procedures

A series of (1-x)SBT-xNBN (x = 0, 0.02, 0.04, 0.06, 0.08, 0.1) ceramics were synthesized by conventional solid-state reaction method. Reagent-grade SrCO₃ (Xilong scientific, 99.00%), Bi₂O₃ (Xilong scientific, 99.00%), Na₂CO₃ (Xilong scientific, 99.98%), TiO₂ (Zhongxing electronic, 99.00%) and Nb₂O₅ (Sinopharm, 99.50%) powders were weighted according to stoichiometric ratios, and then were mixed with ethanol alcohol and zirconia balls by ball milling for 24 h. After drying, the milled powders were calcined at 860 for 3 h in air. The formation reaction was listed as follow:



Then the calcined powders were granulated with 8 wt% of polyvinyl alcohol (PVA) as binders. The granulated particles were pressed

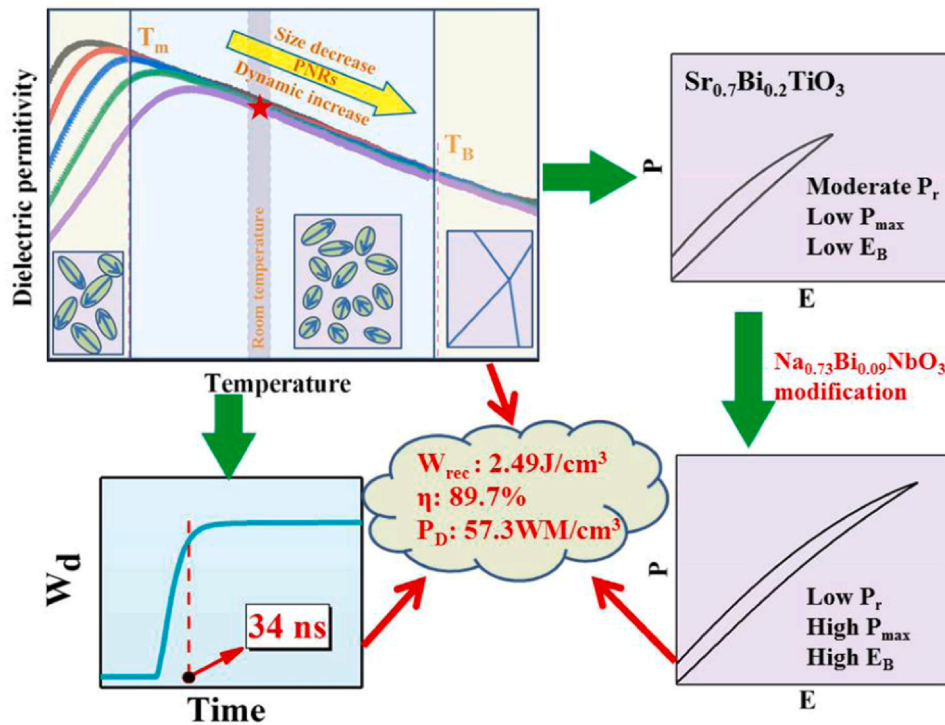


Fig. 1. Schematic diagram of the strategy to obtain high energy storage properties and extremely fast discharge speed.

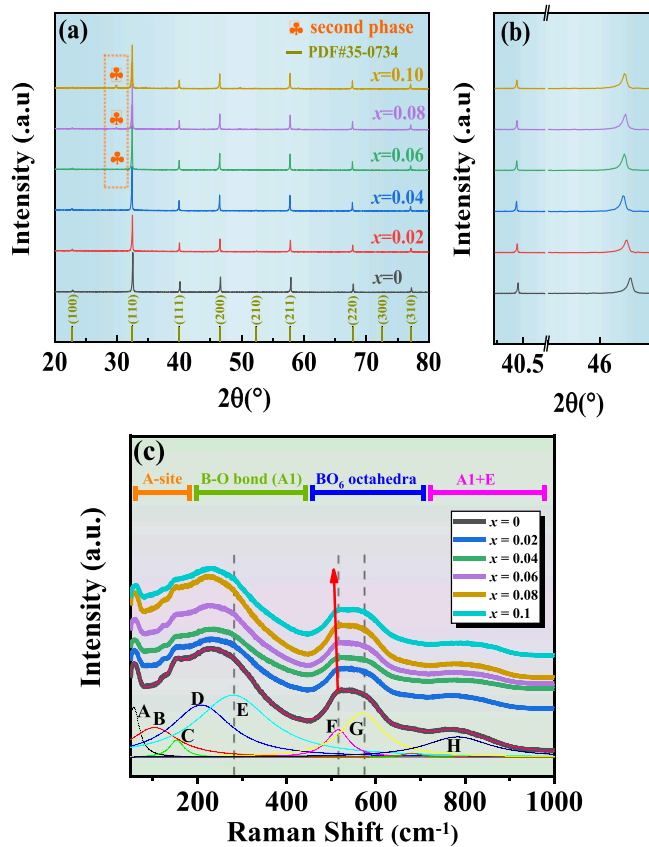


Fig. 2. Room-temperature XRD patterns of $(1-x)$ SBT- x NBN ceramics with 2θ ranging over (a) 20° – 80° (b) 42° – 48° . (c) Room-temperature Raman spectrum for $(1-x)$ SBT- x NBN ceramics.

into disks with a diameter of 12 mm under an axial pressure of 100 MPa. The binders were burned out at 600°C for 2 h, followed by sintering the samples at 1250°C for 3 h in air. The pellets were embedded in the corresponding powders during sintering to prevent the loss of volatile bismuth and sodium.

The crystalline phase was detected by X-ray diffraction (XRD, Bruker, D8-2-advance) with the $\text{Cu K}\alpha$ radiation. Room-temperature Raman spectra were measured by a Horiba Lab-Ram iHR550 spectrometer. The microstructure and compositions of the samples were observed using a field-emission scanning electron microscopy (SEM) (FEG-450, FEI, USA) with elemental mapping. The dielectric properties were obtained by using an LCR meter (Keysight, 4980 A) with the temperature ranging from -100 – 200°C . The ferroelectric properties were measured using a ferroelectric test system (TF ANALYZER 2000HS, aixACCT Systems GmbH, Aachen, Germany). The charge-discharge properties were investigated through a capacitor charge-discharge system (CFD-003, Gogo Instrument, China).

3. Results and discussion

Fig. 2(a) displays the XRD patterns of $(1-x)$ SBT- x NBN ceramics recorded at room temperature. Clearly, the $(1-x)$ SBT- x NBN ceramics

exhibit a single perovskite structure with no apparent trace of the impurities when $x=0$ – 0.04 . It suggests that NBN are dissolved into the matrix lattice of SBT and formed a single solid solution. However, the peaks of second phase (Titanium Oxide Ti_6O_{11}) are found when x exceeds 0.04. There is no splitting of (200) and (111) peaks for $(1-x)$ SBT- x NBN ceramics. It corresponds to a pseudo-cubic phase of all the samples (Fig. 2(b)). The room-temperature Raman spectroscopy, which can probe a local ionic configuration with short length scale, is carried out to further detect the structure evolution of $(1-x)$ SBT- x NBN ceramics [20,21]. Raman spectrum is conducted from 50 to 1000 cm^{-1} range, as shown in Fig. 2(c). The peaks from A to G are fitted by the Lorentz function for $x=0$ sample. Four main vibrations can be discerned [22]. The vibration of A-site ions including Bi, Na and Sr ions in perovskite is below 200 cm^{-1} . The modes between 200 and 400 cm^{-1} are related to B-site and oxygen ions. It can be seen that the mode D becomes broader and mode E is gradually separated from D, the two modes shift apart from each other. The vibrations of BO_6 oxygen octahedron is between 450 and 700 cm^{-1} [22,23]. The modes become broaden and shift toward to low frequency, representing a change in the structure of perovskite with increasing NBN contents. The superposition for all vibration effects is shown over 700 cm^{-1} [22].

Fig. 3(a)–(f) show the typical surface morphology of $(1-x)$ SBT- x NBN ceramics, and a dense microstructure with little pores can be found. The average grain size of the $(1-x)$ SBT- x NBN ceramics increase from $1.8\text{ }\mu\text{m}$ to $3.44\text{ }\mu\text{m}$, with the x increase from 0 to 0.04. This phenomenon shows that NBN doping in SBT can promote the growth of grains, and can be explained as the inevitable volatilization of bismuth and sodium during the high sintering temperature, which results in V''_{Na} and V''_{Bi} , thus the oxygen vacancies would be generated to sustain the overall electrical neutrality [24,25]. The oxygen vacancies are beneficial to mass transportation during sintering [25]. A notable characteristic of the micrographs with inhomogeneous spherical grains combined with rod-like grains is observed in the grain boundaries, with x exceeding 0.04, as shown in Fig. 3(d)–(f). The energy dispersive spectrometer (EDS) analysis of 0.9SBT-0.1NBN ceramic shown in Fig. 3 reveals that the rod-like inclusion has higher signal intensities in Ti and O, indicating the secondary phase is a Ti-enriched phase, which is consistent with the XRD results.

Fig. 4 displays the room-temperature frequency dependence of the dielectric permittivity (ϵ_r) and dielectric loss ($\tan\delta$) of $(1-x)$ SBT- x NBN ceramics, indicating excellent frequency stability of dielectric properties in the frequency range from 100 Hz to 1 MHz. The dielectric constants of samples increase firstly and experience a decline process with the increasing contents of NBN. Furthermore, the dielectric loss is always kept at a low value (<0.01), which benefits to energy storage properties.

Fig. 5(a)–(f) present the temperature dependence of ϵ_r and $\tan\delta$ for $(1-x)$ SBT- x NBN ceramics. The maximum dielectric permittivity ϵ_m temperature (T_m) for $(1-x)$ SBT- x NBN ceramics are lower than room temperature (T_{room}), demonstrating an ergodic relaxor behavior for all samples. Besides, a typical relaxor behavior is observed in $(1-x)$ SBT- x NBN ceramics and proved by the broadening and frequency dispersion of dielectric peaks [11]. The modified Curie-Weiss law is conducted to confirm the relaxor behavior of $(1-x)$ SBT- x NBN ceramics, and the equation is given below:

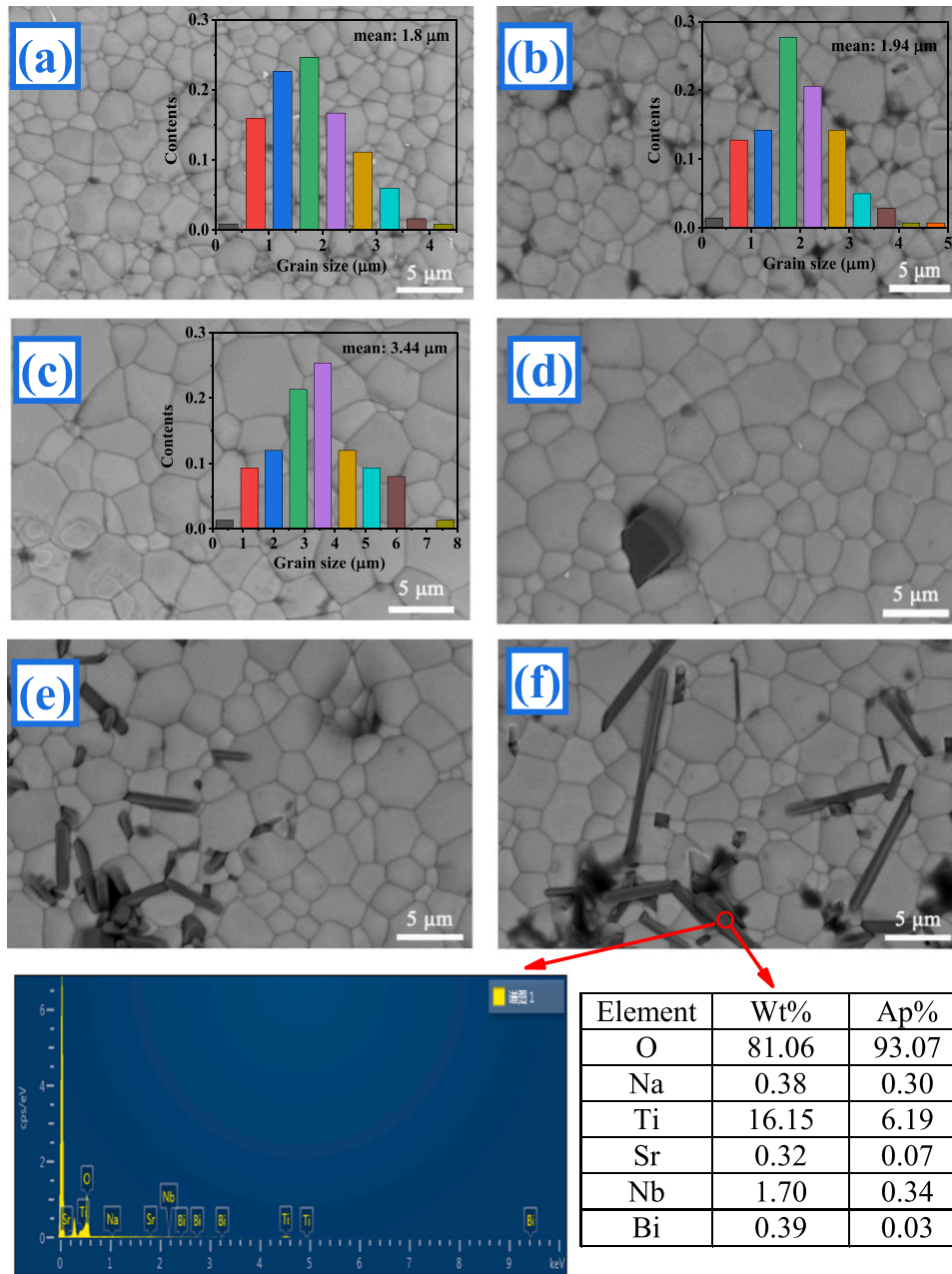


Fig. 3. The SEM images of fresh surface for (1-x)SBT-xNBN ceramics, accompanied with EDS mapping for 0.9SBT-0.1NBN ceramics.

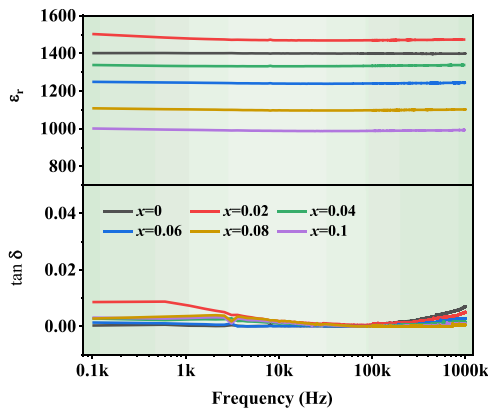


Fig. 4. Frequency-dependent dielectric properties of the (1-x)SBT-xNBN ceramics.

$$\frac{1}{\varepsilon} - \frac{1}{\varepsilon_m} = \frac{(T - T_m)\gamma}{C}, \quad T > T_m \quad (6)$$

where ε_m is the maximum value of dielectric constant, T_m is the temperature for ε_m , C is the Curie-Weiss constant and γ reveals the degree of relaxor. The γ value range between 1 (typical ferroelectric) and 2 (complete relaxor ferroelectric) [2]. It can be seen in Fig. 6(a)-(f), the linear relationship of $\ln(1/\varepsilon - 1/\varepsilon_m)$ and $\ln(T-T_m)$ can be found in all the contents, accompanied with γ ranging between 1.77 and 1.48, demonstrating a powerful relaxor trait. Nevertheless, sometimes the γ value may not indicates the relaxor behavior well, for its value strongly depends on extrinsic defects, such as the homogeneity of composition [7]. Therefore, another method is conducted to further confirm the relaxor behavior, and we define a parameter $\Delta T_{relaxor}$ to quantify the frequency dispersion, which can be defined as follow [7,26].

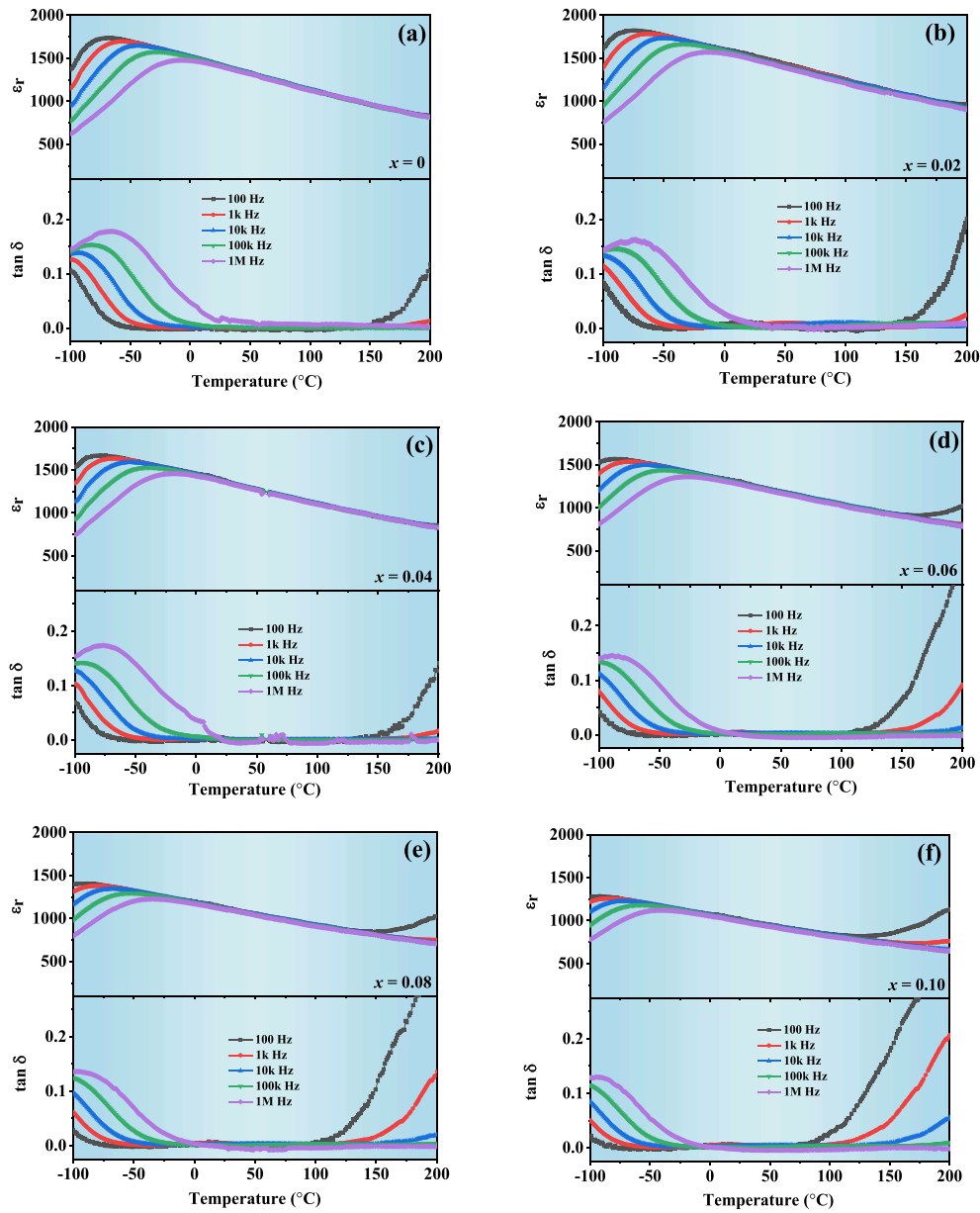


Fig. 5. Temperature-dependent ϵ_r and $\tan\delta$ of $(1-x)\text{SBT}-x\text{NBN}$ ceramics.

$$T_{\text{relaxor}} = T_{\epsilon_m(1 \text{ MHz})} - T_{\epsilon_m(1 \text{ kHz})} \quad (7)$$

where $T_{\epsilon_m(1 \text{ MHz})}$ is the temperature for ϵ_m at 1 MHz and $T_{\epsilon_m(1 \text{ kHz})}$ is the temperature for ϵ_m at 1 kHz. The T_m , γ and calculated $\Delta T_{\text{relaxor}}$ values for $(1-x)\text{SBT}-x\text{NBN}$ ceramics are integrated into Fig. 7, from which we can find that $\Delta T_{\text{relaxor}}$ almost unchanged when $x \leq 0.04$, while it decreases with $x > 0.04$, suggesting a reducing relaxor characteristics. In addition, it can be found that the T_m of $(1-x)\text{SBT}-x\text{NBN}$ ceramics shift to lower temperature with increasing of NBN contents. Thus the correlation between PNRs became weaker,

together with smaller volume of PNRs, which is favorable for charge-discharge properties.

The energy storage properties of the $(1-x)\text{SBT}-x\text{NBN}$ ceramics are investigated using P-E loops, which are conducted at 150 kV/cm and 5 Hz (Fig. 8(a)). The P-E loops become more and more pinched with the addition of NBN, which indicates the decreasing of ferroelectricity. Fig. 8(b) displays the current density (I-E) curves for $(1-x)\text{SBT}-x\text{NBN}$ ceramics. No obvious current peaks can be detected, confirming the ergodicity [5], which is consistent with the results of temperature dependent dielectric constant (Fig. 4). The evolution of

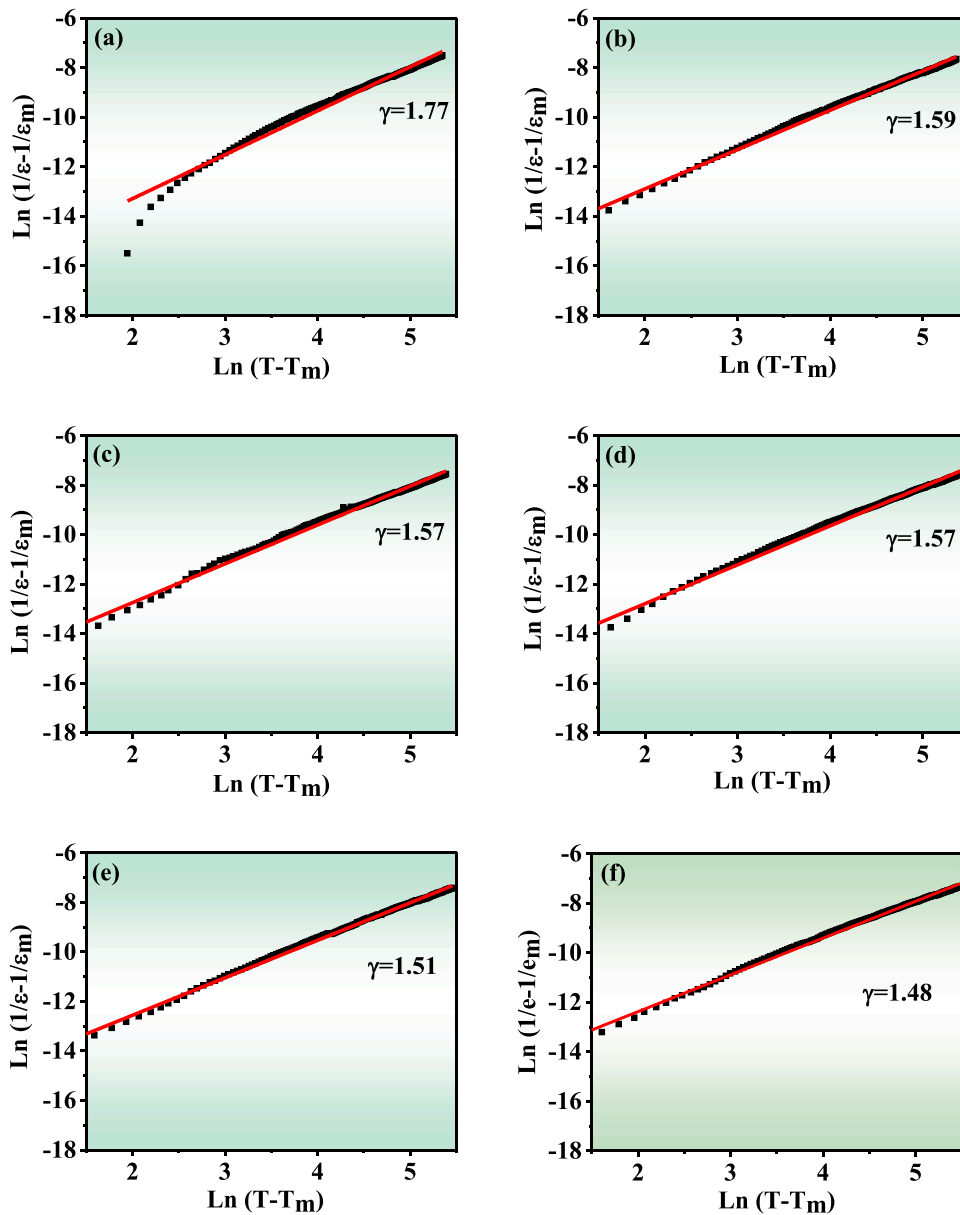


Fig. 6. The curves of $\ln(1/\epsilon-1/\epsilon_m)$ as a function of $\ln(T-T_m)$ for the $(1-x)\text{SBT}-x\text{NBN}$ ceramics at 1 MHz.

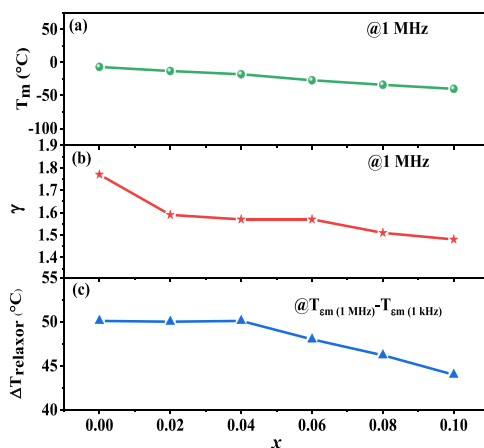


Fig. 7. (a)-(c) T_m , γ , $\Delta T_{\text{relaxor}}$ values as a function of x for $(1-x)\text{SBT}-x\text{NBN}$ ceramics, respectively.

P_{max} , P_r and ΔP ($P_{\text{max}} - P_r$) are shown in Fig. 8(c). The P_{max} and P_r decrease with the increase of x . Additionally, P_r decreases sharply when $x \leq 0.04$, while it almost unchanged when $x > 0.04$. As a result, a high ΔP can be achieved when $x = 0.04$, demonstrating a promising for energy storage properties. Furthermore, it should be noticed that the 0.96SBT-0.04NBN ceramics possess moderate ϵ_r of ~ 1360 and low $\tan\delta$ of ~ 0.002 at room temperature, which are favorable for high E_B .

Room-temperature unipolar P-E loops measured at various electric fields and 5 Hz are used to illustrate the energy storage properties of 0.96SBT-0.04NBN ceramics, as presented in Fig. 9(a). The 0.96SBT-0.04NBN ceramics show slim P-E loops with high P_{max} and negligible P_r under different electric fields, which are benefit to enhance energy storage properties. To qualify the energy storage properties, we summarize the W_{rec} , W_{tot} , W_{loss} , as well as η under different electric fields, as shown in Fig. 9(b). It can be seen that W_{rec} and W_{tot} are improved obviously with enhancing electric field, while W_{loss} increases slightly. Furthermore, the η decreases with enhancing electric field due to the large hysteresis of P-E loop at high

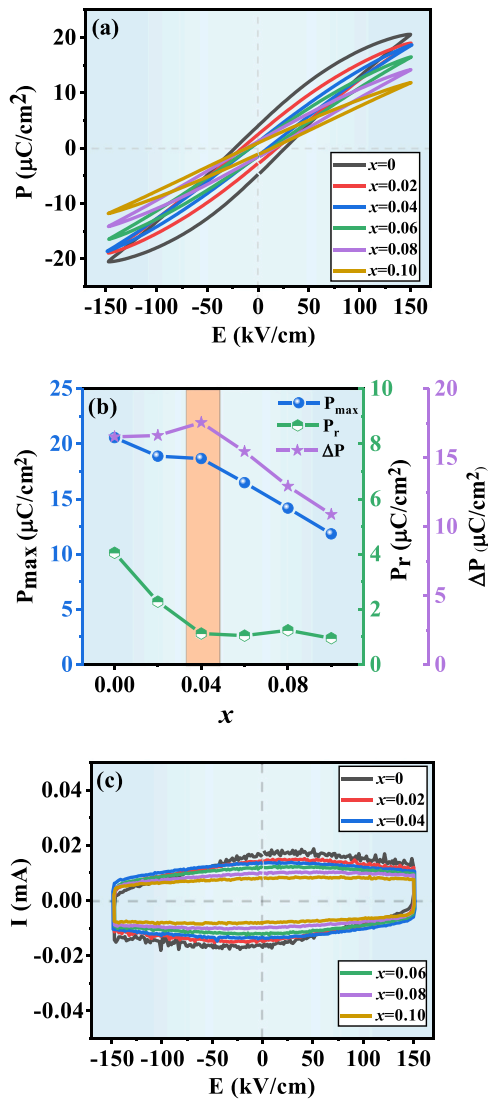


Fig. 8. (a) P-E loops of (1-x)SbT-xNBN ceramics at 150 kV/cm and 5 Hz. (b) Corresponding P_{max}, P_r and ΔP (P_{max} - P_r) values as a function of x. (c) I-E curves of (1-x)SbT-xNBN ceramics at 150 kV/cm and 5 Hz.

electric field. It is well accepted that the formation of long-range polar ordering through domain switching can be induced by a high enough electric field [5]. Especially, a combination of excellent energy storage properties for 0.96SbT-0.04NBN ceramics was achieved at 250 kV/cm ($W_{rec} = 2.49 \text{ J/cm}^3$, $\eta = 89.7\%$).

For the practical application in dielectric capacitors, large W_{rec} and high η , together with their excellent thermal stability and frequency stability are required. Fig. 10(a) displays the temperature-dependent unipolar P-E loops of 0.96SbT-0.04NBN ceramics in the temperature range from 25 °C to 125 °C at 100 kV/cm and 5 Hz. It is

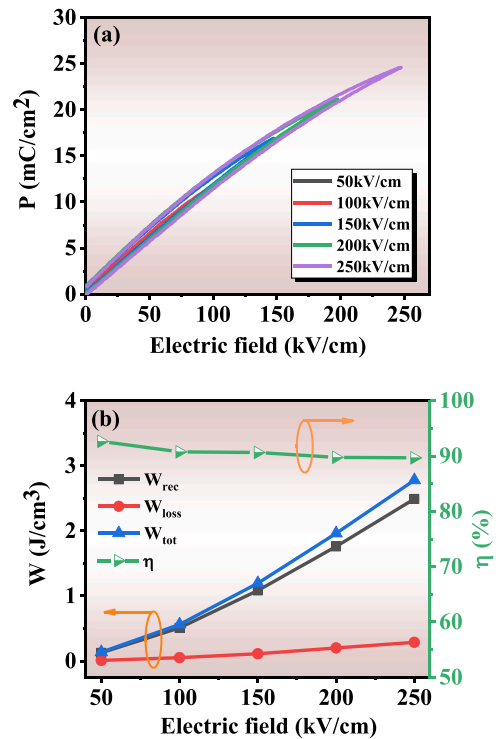


Fig. 9. (a) Unipolar P-E loops of 0.96SbT-0.04NBN ceramics with different electric fields at 5 Hz and ambient temperature. (c) I-E loops of 0.96SbT-0.04NBN ceramics. (b) W_{rec} , W_{loss} , W_{tot} and η of 0.96SbT-0.04NBN ceramics.

evident that the 0.96SbT-0.04NBN ceramics maintain slim P-E loops over the whole temperature range. When the temperature increases from 25 °C to 125 °C, the P_{max} diminishes from 11.64 μC/cm² to 9.57 μC/cm², accompanied by negligible P_r (~0 μC/cm²). These characteristic are related to the relaxor behavior of 0.96SbT-0.04NBN ceramics, as mentioned above. Fig. 10(b) depicts the W_{rec} and η as a function of different temperature, which show sound stability in this temperature range (W_{rec} : 0.52–0.43 J/cm³, η : 92–90%). The excellent temperature stability of the W_{rec} and η for 0.96SbT-0.04NBN ceramics may attribute to the neighboring PNRs coupling which can only occur under high electric field and low temperature [27]. The unipolar frequency dependence of P-E loops for 0.96SbT-0.04NBN ceramics measured at 100 kV/cm and room temperature are represented in Fig. 10(c), the corresponding energy storage properties are depicted in Fig. 10(d). The slight fluctuations of W_{rec} and η confirm the frequency-insensitivity characteristic of 0.96SbT-0.04NBN ceramics in this frequency range. For example, the W_{rec} is 0.55 J/cm³ at 1 Hz and 0.53 J/cm³ at 100 Hz. Besides, the η which always more than 85% are achieved, indicating a good frequency stability of energy storage properties.

Fig. 11(a) displays the room-temperature overdamped pulse discharge current waveforms of 0.96SbT-0.04NBN ceramics, in which the current reaches the peak in a short time, and the

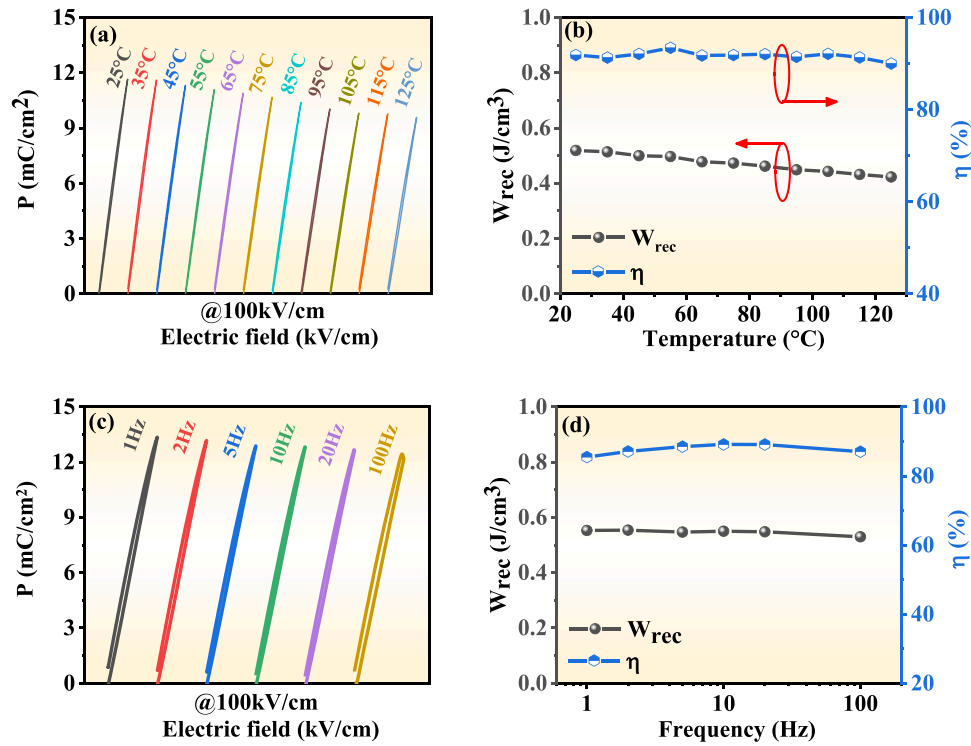


Fig. 10. Unipolar P-E loops of 0.96SBT-0.04NBN ceramics at different temperature (a) and different frequencies (c) at 100 kV/cm. (b) and (d) The corresponding calculated W_d and η vs temperature and frequency, respectively.

discharge process lasts less than 100 ns. According to the curves, the discharge energy density (W_d) can be obtained by the following formula:

$$W_d = R \int i(t)^2 dt / V \quad (8)$$

where R is the total load resistor ($R = 120 \Omega$), $i(t)$ is the discharge current obtained by using the oscillograph, and V represents the sample volume [28,29]. As displayed in Fig. 11(b), the W_d increases from 0.20 J/cm³ at 60 kV/cm to 0.77 J/cm³ at 120 kV/cm. In addition, W_d reaches the maximum value in an extremely short time, and $\tau_{0.9}$ is introduced to confirm the discharge speed, which is defined as the time to achieve 90% of the final value [29]. The remarkable $\tau_{0.9}$ of 34 ns for 0.96SBT-0.04NBN ceramics demonstrating its high potential for fast pulse power applications. Fig. 11(c) presents the underdamped discharge curves for 0.96SBT-0.04NBN ceramics at various electric fields and room temperature. With the enhancement of electric field, the first current peak increases gradually. Based on the obtained underdamped discharge waveforms, the maximum current (I_{max}), calculated current density ($C_D = I_{max}/S$) and power density ($P_D = EI_{max}/2S$) are plotted in the Fig. 11(d) [5]. It can be found that the I_{max} , C_D and P_D monotonously increase from 15.0 A, 477.7 A/cm² and 14.3 MW/cm³ to 30.0 A, 955.4 A/cm² and 57.3 MW/cm³, respectively,

with increasing electric field from 60 kV/cm to 120 kV/cm. According to the equation:

$$C_D = \frac{I_{max}}{S} = \frac{dQ_{max}}{S dt} = \frac{dP_{max}}{dt} \quad (9)$$

the large C_D of 0.96SBT-0.04NBN ceramics can be attributed to the high induced polarization and short discharge time [5]. Besides, the large electric field of 120 kV/cm is also responsible for the large P_D of 0.96SBT-0.04NBN ceramics. These results reveal the prospect of 0.96SBT-0.04NBN ceramics for application in pulsed power technology.

Fig. 12(a) and (b) exhibit intuitive comparisons of energy storage properties [7,14–16,19,27,28,30–40] and charge-discharge performance [8,41–47] for 0.96SBT-0.04NBN ceramics and other reported ceramics. Most of the previously reported ceramics exhibit a common minus that the trade-off between W_{rec} and η . Note that the brand-new 0.96SBT-0.04NBN ceramics show a large W_{rec} (2.49 J/cm³) and a high η (89.7%) simultaneously, which is superior to other ceramics. Besides, 0.96SBT-0.04NBN ceramics also possess an ultra-fast discharge speed (~34 ns) combined with a remarkable P_D of 57.3 MW/cm³. These results fully reveal the superiority of 0.96SBT-0.04NBN ceramics in pulse ceramic capacitors.

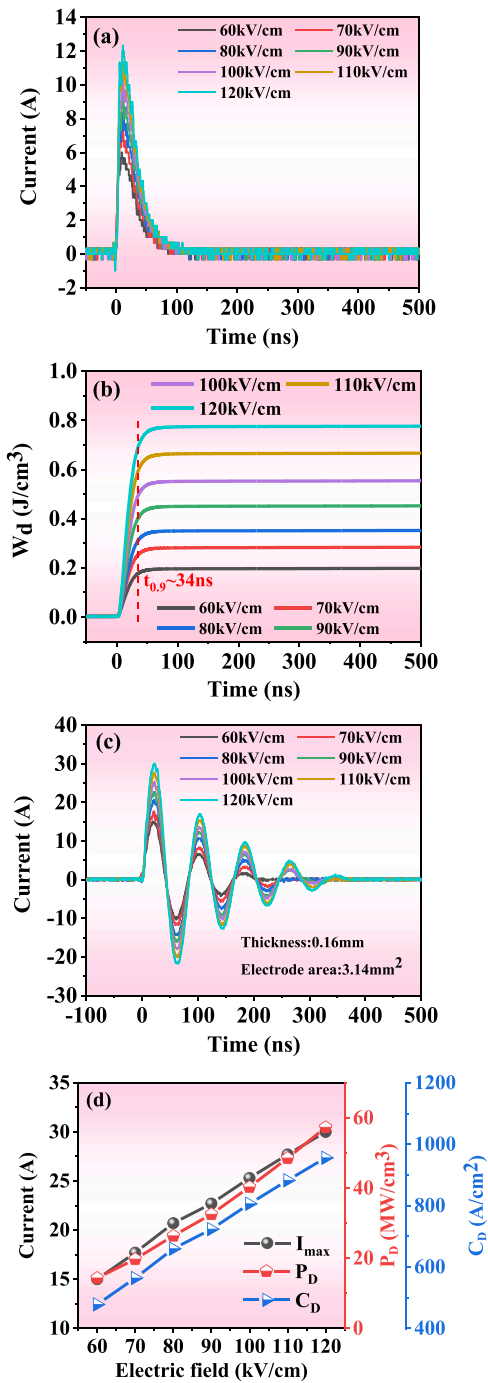


Fig. 11. (a) Overdamped pulse discharge current curves of 0.96SBT-0.04NBN ceramics under various electric fields. (b) W_d as a function of time for 0.96SBT-0.04NBN ceramics. (c) Underdamped discharge waveforms of 0.96SBT-0.04NBN ceramics at different electric fields. (d) Variation of I_{max} , P_D and C_D as a function of electric field.

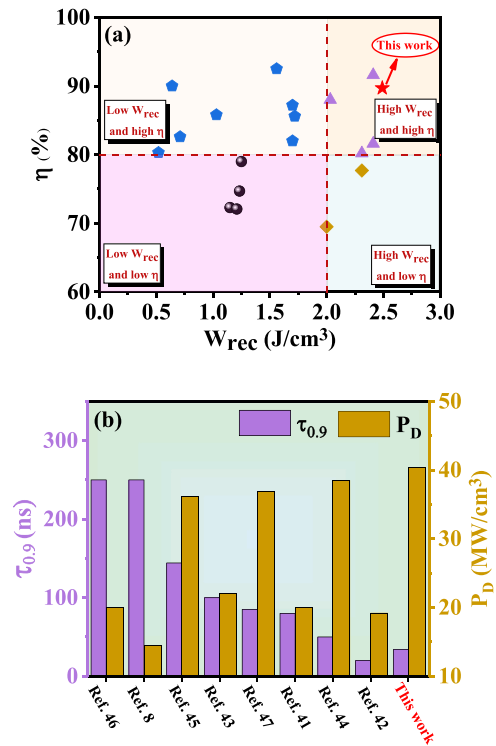


Fig. 12. (a) W_{rec} and η of 0.96SBT-0.04NBN ceramics and some previously published ceramics. (b) A comparison of $\tau_{0.9}$ and P_D for 0.96SBT-0.04NBN ceramics and other reported ceramics.

4. Conclusions

In summary, the $(1-x)SBT-xNBN$ ceramics are studied for energy storage applications. The introduction of NBN into SBT ergodic relaxors lead to the enhanced W_{rec} of $2.49 J/cm^3$ and η of 89.7% at 250 kV/cm for 0.96SBT-0.04NBN ceramics. Besides, the W_{rec} and η of 0.96SBT-0.04NBN ceramics possess excellent thermal stability and frequency stability. More significantly, an extraordinary fast discharge rate of 34 ns and remarkable P_D of $57.3 MW/cm^3$ are obtained, which can be attributed to the high dynamic and weak correlation PNRs in ergodic relaxor ferroelectric state. The notable improvements in energy storage and charge-discharge properties indicate that 0.96SBT-0.04NBN ceramic is a promising candidate for advanced pulsed power applications.

CRediT authorship contribution statement

Kai Yao: Investigation, Methodology, Writing - original draft. **Changrong Zhou:** Funding acquisition, Supervision, Resources, Writing - review & editing. **Jiang Wang:** Investigation, Methodology. **Qingning Li:** Investigation, Methodology. **Changlai Yuan:** Investigation, Methodology. **Jiwen Xu:** Investigation, Methodology. **Guohua Chen:** Investigation, Methodology. **Guanghui Rao:** Supervision, Resources, Writing - review & editing.

Declaration of Competing Interest

The authors declare that they have no known competing financial interests or personal relationships that could have appeared to influence the work reported in this paper.

Acknowledgements

This work was supported by the National Nature Science Foundation of China, China (51862004) and the Natural Science Foundation of Guangxi, China (2018GXNSFAA294039, 2017GXNSFDA198024, 2017GXNSFAA198339).

References

- W. Ma, Y. Zhu, M. Marwat, P. Fan, B. Xie, D. Salamon, Z. Ye, H. Zhang, Enhanced energy-storage performance with excellent stability under low electric fields in BNT-ST relaxor ferroelectric ceramics, *J. Mater. Chem. C* 7 (2019) 281–288.
- Y. Wu, Y. Fan, N. Liu, P. Peng, M. Zhou, S. Yan, F. Cao, X. Dong, G. Wang, Enhanced energy storage properties in sodium bismuth titanate-based ceramics for dielectric capacitor applications, *J. Mater. Chem. C* 7 (2019) 6222–6230.
- H. Zhang, T. Wei, Q. Zhang, W. Ma, P. Fan, D. Salamon, S. Zhang, B. Nan, H. Tan, Z. Ye, A review on the development of lead-free ferroelectric energy-storage ceramics and multilayer capacitors, *J. Mater. Chem. C* 8 (2020) 16648–16667.
- M. Zhou, R. Liang, Z. Zhou, X. Dong, Superior energy storage properties and excellent stability of novel NaNbO_3 -based lead-free ceramics with A-site vacancy obtained via a Bi_2O_3 substitution strategy, *J. Mater. Chem. A* 6 (2018) 17896–17904.
- X. Zhou, H. Qi, Z. Yan, G. Xue, H. Luo, D. Zhang, Superior thermal stability of high energy density and power density in domain-engineered $\text{Bi}_{0.5}\text{Na}_{0.5}\text{TiO}_3$ - NaTaO_3 relaxor ferroelectrics, *ACS Appl. Mater. Interfaces* 11 (2019) 43107–43115.
- H. Pan, F. Li, Y. Liu, Q. Zhang, Ultrahigh-energy density lead-free dielectric films via polymorphic nanodomain design, *Science* 365 (2019) 578–582.
- H. Yang, F. Yan, Y. Lin, T. Wang, F. Wang, Y. Wang, L. Guo, W. Tai, H. Wei, Lead-free BaTiO_3 - $\text{Bi}_{0.5}\text{Na}_{0.5}\text{TiO}_3$ - $\text{Na}_{0.7}\text{Bi}_{0.09}\text{NbO}_3$ relaxor ferroelectric ceramics for high energy storage, *J. Eur. Ceram. Soc.* 37 (2017) 3303–3311.
- Z. Chen, X. Bu, B. Ruan, J. Du, P. Zheng, L. Li, F. Wen, W. Bai, W. Wu, L. Zheng, Y. Zhang, Simultaneously achieving high energy storage density and efficiency under low electric field in BiFeO_3 -based lead-free relaxor ferroelectric ceramics, *J. Eur. Ceram. Soc.* 40 (2020) 5450–5457.
- Y. Li, N. Sun, X. Li, J. Du, L. Chen, H. Gao, X. Hao, M. Cao, Multiple electrical response and enhanced energy storage induced by unusual coexistent-phase structure in relaxor ferroelectric ceramics, *Acta Mater.* 146 (2018) 202–210.
- P. Zhao, B. Tang, F. Si, C. Yang, H. Li, S. Zhang, Novel Ca doped $\text{Sr}_{0.7}\text{Bi}_{0.2}\text{TiO}_3$ lead-free relaxor ferroelectrics with high energy density and efficiency, *J. Eur. Ceram. Soc.* 40 (5) (2020) 1938–1946.
- M. Sakurai, K. Kanehara, H. Takeda, T. Tsurumi, T. Hoshi, Wideband dielectric spectroscopy of $(\text{Sr}_{0.7}\text{Bi}_{0.2})\text{TiO}_3$ ceramics and its microscopic mechanism of polarization, *J. Ceram. Soc. Jpn.* 124 (2016) 664–667.
- G. Zhang, M. Cao, H. Hao, H. Liu, Energy storage characteristics in $\text{Sr}_{(1-1.5x)}\text{Bi}_x\text{TiO}_3$ ceramics, *Ferroelectrics* 447 (2013) 86–94.
- M. Chao, J. Liu, M. Zeng, D. Wang, H. Yu, Y. Yuan, S. Zhang, High discharge efficiency of $(\text{Sr}, \text{Pb}, \text{Bi})\text{TiO}_3$ relaxor ceramics for energy-storage application, *Appl. Phys. Lett.* 112 (2018) 203903.
- P. Ren, Z. Liu, X. Wang, Z. Duan, Y. Wan, F. Yan, G. Zhao, Dielectric and energy storage properties of SrTiO_3 and SrZrO_3 modified $\text{Bi}_{0.5}\text{Na}_{0.5}\text{TiO}_3$ - $\text{Sr}_{0.8}\text{Bi}_{0.1}\text{TiO}_3$ based ceramics, *J. Alloy. Comp.* 742 (2018) 683–689.
- Q. Li, Z. Yao, L. Ning, S. Gao, B. Hu, G. Dong, H. Fan, Enhanced energy-storage properties of $(1-x)(0.7\text{Bi}_{0.5}\text{Na}_{0.5}\text{TiO}_3-0.3\text{Bi}_{0.2}\text{Sr}_{0.7}\text{TiO}_3)$ - $x\text{NaNbO}_3$ lead-free ceramics, *Ceram. Int.* 44 (2018) 2782–2788.
- D. Hu, Z. Pan, Z. He, F. Yang, Significantly improved recoverable energy density and ultrafast discharge rate of $\text{Na}_{0.5}\text{Bi}_{0.5}\text{TiO}_3$ -based ceramics, *Ceram. Int.* 46 (2020) 15364–15371.
- Q. Xu, M.T. Lanagan, X. Huang, J. Xie, L. Zhang, H. Hao, H. Liu, Dielectric behavior and impedance spectroscopy in lead-free BNT-BT-NBN perovskite ceramics for energy storage, *Ceram. Int.* 42 (2016) 9728–9736.
- H. Yang, F. Yan, Y. Lin, T. Wang, F. Wang, High energy storage density over a broad temperature range in sodium bismuth titanate-based lead-free ceramics, *Sci. Rep.* 7 (2017) 8726.
- J. Wang, H. Fan, B. Hu, H. Jiang, Enhanced energy-storage performance and temperature-stable dielectric properties of $(1-x)(0.94\text{Na}_{0.5}\text{Bi}_{0.5}\text{TiO}_3-0.06\text{BaTiO}_3)$ - $x\text{Na}_{0.7}\text{Bi}_{0.09}\text{NbO}_3$ ceramics, *J. Mater. Sci. Mater. Electron.* 30 (2018) 2479–2488.
- X. Jiang, B. Wang, L. Luo, W. Li, J. Zhou, H. Chen, Electrical properties of $(1-x)(\text{Bi}_{0.5}\text{Na}_{0.5}\text{TiO}_3-x\text{KNbO}_3)$ lead-free ceramics, *J. Solid State Chem.* 213 (2014) 72–78.
- B. Wylie-van Eerd, D. Damjanovic, N. Klein, N. Setter, J. Trodahl, Structural complexity of $(\text{Na}_{0.5}\text{Bi}_{0.5})\text{TiO}_3$ - BaTiO_3 as revealed by Raman spectroscopy, *Phys. Rev. B* 82 (2010).
- B. Yan, H. Fan, A.K. Yadav, C. Wang, Z. Du, M. Li, W. Wang, W. Dong, S. Wang, $(\text{Bi}_{0.50}\text{Na}_{0.40}\text{K}_{0.10})_{0.94}\text{Ba}_{0.06}]_{1-x}\text{La}_x\text{Ti}_{0.975}\text{Ta}_{0.025}\text{O}_3$ lead-free relaxor ceramics with high energy storage density and thermally stable dielectric properties, *J. Mater. Sci.* 55 (2020) 14728–14739.
- W. Bai, P. Li, L. Li, J. Zhang, B. Shen, J. Zhai, Structure evolution and large strain response in BNT-BT lead-free piezoceramics modified with $\text{Bi}(\text{Ni}_{0.5}\text{Ti}_{0.5})\text{O}_3$, *J. Alloy. Comp.* 649 (2015) 772–781.
- H. Yang, F. Yan, Y. Lin, T. Wang, Enhanced recoverable energy storage density and high efficiency of SrTiO_3 -based lead-free ceramics, *Appl. Phys. Lett.* 111 (2017) 253903.
- Q. Xu, H. Liu, L. Zhang, J. Xie, H. Hao, M. Cao, Z. Yao, M.T. Lanagan, Structure and electrical properties of lead-free $\text{Bi}_{0.5}\text{Na}_{0.5}\text{TiO}_3$ -based ceramics for energy-storage applications, *RSC Adv.* 6 (2016) 59280–59291.
- Z. Yu, C. Ang, R. Guo, A.S. Bhalla, Ferroelectric-relaxor behavior of $\text{Ba}(\text{Ti}_{0.7}\text{Zr}_{0.3})\text{O}_3$ ceramics, *J. Appl. Phys.* 92 (2002) 2655–2657.
- M. Zhou, R. Liang, Z. Zhou, X. Dong, Novel BaTiO_3 -based lead-free ceramic capacitors featuring high energy storage density, high power density, and excellent stability, *J. Mater. Chem. C* 6 (2018) 8528–8537.
- W. Li, D. Zhou, L. Pang, R. Xu, H. Guo, Novel barium titanate based capacitors with high energy density and fast discharge performance, *J. Mater. Chem. A* 5 (2017) 19607–19612.
- X. Qiao, D. Wu, F. Zhang, B. Chen, X. Ren, P. Liang, H. Du, X. Chao, Z. Yang, $\text{Bi}_{0.5}\text{Na}_{0.5}\text{TiO}_3$ -based relaxor ferroelectric ceramic with large energy density and high efficiency under a moderate electric field, *J. Mater. Chem. C* 7 (2019) 10514–10520.
- J. Wu, A. Mahajan, L. Riekehr, H. Zhang, B. Yang, N. Meng, Z. Zhang, H. Yan, Perovskite $\text{Sr}_x(\text{Bi}_{1-x}\text{Na}_{0.97-x}\text{La}_{0.03})_{0.5}\text{TiO}_3$ ceramics with polar nano regions for high power energy storage, *Nano Energy* 50 (2018) 723–732.
- N. Qu, H. Du, X. Hao, A new strategy to realize high comprehensive energy storage properties in lead-free bulk ceramics, *J. Mater. Chem. C* 7 (2019) 7993–8002.
- J. Sui, H. Fan, B. Hu, L. Ning, High temperature stable dielectric properties and enhanced energy-storage performance of $(1-x)(0.85\text{Na}_{0.5}\text{Bi}_{0.5}\text{TiO}_3-0.15\text{Ba}_{0.8}\text{Ca}_{0.2}\text{Ti}_{0.8}\text{Zr}_{0.2}\text{O}_3)$ - $x\text{K}_{0.5}\text{Na}_{0.5}\text{NbO}_3$ lead-free ceramics, *Ceram. Int.* 44 (2018) 18054–18059.
- B. Hu, H. Fan, L. Ning, Y. Wen, C. Wang, High energy storage performance of $(\text{Bi}_{0.5}\text{Na}_{0.5})_{0.94}\text{Ba}_{0.06}]_{0.97}\text{La}_{0.03}\text{Ti}_{1-x}(\text{Al}_{0.5}\text{Nb}_{0.5})\text{O}_3$ ceramics with enhanced dielectric breakdown strength, *Ceram. Int.* 44 (2018) 15160–15166.
- F. Li, R. Si, T. Li, C. Wang, J. Zhai, High energy storage performance and fast discharging speed in dense $0.7\text{Bi}_{0.5}\text{K}_{0.5}\text{TiO}_3-0.3\text{SrTiO}_3$ ceramics via a novel rolling technology, *Ceram. Int.* 46 (2020) 6995–6998.
- Y. Pu, M. Yao, L. Zhang, P. Jing, High energy storage density of $0.55\text{Bi}_{0.5}\text{Na}_{0.5}\text{TiO}_3-0.45\text{Ba}_{0.85}\text{Ca}_{0.15}\text{Ti}_{0.9}\text{Zr}_{0.1}\text{SnO}_3$ ceramics, *J. Alloy. Comp.* 687 (2016) 689–695.
- Z. Yang, F. Gao, H. Du, L. Jin, L. Yan, Q. Hu, Y. Yu, S. Qu, X. Wei, Z. Xu, Y. Wang, Grain size engineered lead-free ceramics with both large energy storage density and ultrahigh mechanical properties, *Nano Energy* 58 (2019) 768–777.
- B. Yan, H. Fan, A.K. Yadav, C. Wang, X. Zheng, H. Wang, W. Wang, W. Dong, S. Wang, Enhanced energy-storage performance and thermally stable permittivity for $\text{K}_{0.5}\text{Na}_{0.5}\text{NbO}_3$ modified $(\text{Na}_{0.5}\text{Bi}_{0.5})_{0.84}\text{Sr}_{0.16}]_{0.98}\text{La}_{0.01}\text{TiO}_3$ lead-free perovskite ceramics, *Ceram. Int.* 46 (2020) 9637–9645.
- Z. Yu, Y. Liu, M. Shen, H. Qian, F. Li, Y. Lyu, Enhanced energy storage properties of BiAlO_3 modified $\text{Bi}_{0.5}\text{Na}_{0.5}\text{TiO}_3$ - $\text{Bi}_{0.5}\text{K}_{0.5}\text{TiO}_3$ lead-free antiferroelectric ceramics, *Ceram. Int.* 43 (2017) 7653–7659.
- J. Wang, C. Zhou, Q. Li, W. Zeng, J. Xu, G. Chen, C. Yuan, G. Rao, Dual relaxation behaviors and large electrostrictive properties of $\text{Bi}_{0.5}\text{Na}_{0.5}\text{TiO}_3$ - $\text{Sr}_{0.85}\text{Bi}_{0.1}\text{TiO}_3$ ceramics, *J. Electron. Mater.* 53 (2018) 8844–8854.
- Z. Shen, X. Wang, B. Luo, L. Li, BaTiO_3 - BiYbO_3 relaxor materials for energy storage applications, *J. Mater. Chem. A* 3 (2015) 18146–18153.
- L. Zhang, Y. Pu, M. Chen, Ultra-high energy storage performance under low electric fields in $\text{Na}_{0.5}\text{Bi}_{0.5}\text{TiO}_3$ -based relaxor ferroelectrics for pulse capacitor applications, *Ceram. Int.* 46 (2020) 98–105.
- X. Guo, Y. Pu, W. Wang, J. Ji, J. Li, R. Shi, M. Yang, Ultrahigh energy storage performance and fast charge-discharge capability in Dy-modified SrTiO_3 linear ceramics with high optical transmissivity by defect and interface engineering, *Ceram. Int.* 46 (2020) 21719–21727.
- L. Zhang, Y. Pu, M. Chen, T. Wei, X. Peng, Novel $\text{Na}_{0.5}\text{Bi}_{0.5}\text{TiO}_3$ based, lead-free energy storage ceramics with high power and energy density and excellent high-temperature stability, *Chem. Eng. J.* 383 (2020) 123154.
- R. Shi, Y. Pu, W. Wang, X. Guo, J. Li, M. Yang, S. Zhou, A novel lead-free NaNbO_3 - $\text{Bi}(\text{Zn}_{0.5}\text{Ti}_{0.5})\text{O}_3$ ceramics system for energy storage application with excellent stability, *J. Alloy. Comp.* 815 (2020) 152356.
- D. Li, Y. Lin, Q. Yuan, M. Zhang, L. Ma, H. Yang, A novel lead-free $\text{Na}_{0.5}\text{Bi}_{0.5}\text{TiO}_3$ -based ceramic with superior comprehensive energy storage and discharge properties for dielectric capacitor applications, *J. Mater.* 6 (2020) 743–750.
- Y. Fan, Z. Zhou, R. Liang, X. Dong, Designing novel lead-free NaNbO_3 -based ceramic with superior comprehensive energy storage and discharge properties for dielectric capacitor applications via relaxor strategy, *J. Eur. Ceram. Soc.* 39 (2019) 4770–4777.
- M. Zhou, R. Liang, Z. Zhou, X. Dong, Combining high energy efficiency and fast charge-discharge capability in novel BaTiO_3 -based relaxor ferroelectric ceramic for energy-storage, *Ceram. Int.* 45 (2019) 3582–3590.